THREE-DIMENSIONAL MECHANICS OF EUKARYOTIC FLAGELLA

M. HINES AND J. J. BLUM
Department of Physiology, Duke University Medical Center, Durham, North Carolina 27710

ABSTRACT Equations are derived that account for the contribution of internal structure of cilia and flagella to motion in three dimensions according to a sliding filament model of the motile system. It is shown that for reasonable amounts of bending and twisting, the bending properties of an axoneme can be described by a linear elastic bending resistance, and approximate values for the bending and twisting resistances are computed. Expressions for the shear moments contributed by purely elastic or pinned links between filaments are also derived. It is shown that within the confines of a strict sliding filament model such internal structures cannot by themselves produce twist. Thus planar bending will occur if the internal shear force lies in a plane. Application of an external force, however, will in general produce twisting. Computer simulations of flagellar shape in response to a constant external force applied to the distal end of the axoneme are presented. It is shown that a small amount of twist may arise because of acylindrical bend resistance. Large twists, however, result when the external force is applied to an axoneme with internal shear resistant links.

INTRODUCTION

Flagella and cilia beat with a wide variety of three-dimensional shapes of varying complexity. This variety of shapes contrasts with the rather symmetric organization of the axoneme. Previous attempts to understand how internal components such as dynein arms and outer doublets produce bending waves have focused on those flagella that display planar bending. The planarity encouraged the use of two-dimensional equations for analysis of bend propagation. Such models, of course, beg the question of how a three-dimensional system can produce two-dimensional motion. Even if the properties of the central pair were to define the plane of bending merely by virtue of the extra stiffness along one axis, the possibility of twisting makes it unlikely that beating would be planar. That cilia of the 9 + 0 (Costello et al., 1969), 9 + 1 (Henley et al., 1969), 6 + 0 (Schrevel and Besse, 1975), and 3 + 0 (Prensier et al., 1979) patterns also beat with three-dimensional shapes further emphasizes the importance of understanding the role of internal structure in determining the form of the propagating wave. Preceding theoretical studies of bend formation and bend propagation (see Blum and Hines, 1979, for a recent review) have simplified the 9 + 2 structure by projection of the contributions of the outer doublets onto the plane of bending, so that, in essence, one composite pair of sliding filaments was considered, and bending was necessarily planar. This approach has permitted the development of models of flagellar motility that take into account the presence of passive shear links (e.g., nexin links) and the cyclic attachment-detachment of the dynein arms. A fundamental issue still to be resolved is how bending is coordinated with sliding to yield wave propagation at a specified frequency. The participation of the radial spoke system, at least in 9 + 2 flagella, seems to play an important role in converting sliding into bending (Warner and Satir, 1974), but no details as to how coordination of these processes is achieved are available. That the radial spoke system is a three-dimensional array of elements further emphasizes the need for an investigation of the effects of internal structural organization on flagellar motility.

Although most studies on wave shape in cilia and flagella have tacitly ignored the possibility that twisting occurs, it is now clear that, at least in some circumstances, twisting may be a significant aspect of flagellar motility. From studies on hamster sperm flagella that were arrested by quick freezing, Wooley (1977) concluded that the plane of action of a given bend cycle undergoes twisting as each bend cycle is succeeded by a new bend cycle. He suggested that the preferred plane of bending is determined by peripheral doublet 1, then successive planes by doublets 2, 3, etc. In 6 + 0 and 3 + 0 flagella, each bend seems to stay on its own set of doublets, the next bend being on another set, and twisting has been observed even in a doubly tethered cell (Goldstein et al., 1978). Bradfield (1955) and Costello (1973) have suggested that helical motion may arise from a progression of activity around the circumference of the axoneme as the wave progresses along the axis.

A change in orientation of the central pair during beating was observed by Satir (1968) and by Tamm and Horridge (1970). More recently, Omoto and Kung (1980) have observed twist in the central pair of filaments in *Paramecium* cilia, which they interpret to indicate that the central pair rotates continuously, its rotation originating at

the base of the cilium. Thus there are many indications that twisting of at least some ciliary components occurs during ciliary motion and, indeed, may play a role in determining the three-dimensional motion. The need for a comprehensive analysis of the contribution of internal structure to three-dimensional flagellar mechanics is therefore clear.

In section I of this paper we analyze flagellar shape by developing a formalism that accounts for the change in coordinate axes of each of the filaments in a flagellum for arbitrary bending and twisting, and show how coordinate transformations can be used to keep track of local orientation of the internal components. Section II then formulates the sliding filament model, explicitly allowing for the contribution of each of the outer doublets. A method for computing the bending and twisting resistances of a flagellum is presented in section III. When a central pair is present, the bending resistance encountered in response to an internal dynein-generated force will depend on the angle that the force makes within the central pair cross section. Estimates of the values of the components of the bend resistance matrix are obtained. In section IV we derive general expressions for the moments generated by internal shear forces, and apply these to an analysis of the contribution of nexinlike links. This analysis shows that such elastic links cannot contribute any twisting moment. Section V presents a numerical method for computer analysis of the three-dimensional sliding filament model and simulations of flagellar shape in response to application of a constant external force for various degrees of internal asymmetry. The contribution of internal structure to bend shape and twist is then examined, and conditions for nearly planar bending are discussed.

A brief outline of some of these results has been presented (Hines and Blum, 1982).

NOMENCLATURE

Depending upon the context, a subscript may refer to the filament number, $i = 1, 9$; a component of a vector, $i = 1, 3$; or a discrete point on the flagellum, $p = 1, N$. In the rare case that confusion is possible, the meaning is explicitly stated.

An arrow over a symbol denotes a three-dimensional vector. A circumflex over a symbol denotes a unit vector. Two tildes under a symbol denote a 3×3 matrix.

Symbols that appear in more than one section of the paper are listed below with their units:

$\underset{\sim}{A}$	coordinate transformation
$\underset{\sim}{E}_b$	bending resistance matrix
E_{xx}, E_{yy}, E_{zz}	diagonal components of E_b ($pN\mu m^2$)
E_s	shear force coefficient (pN/μm)
$\vec{\phi}$	external force density (pN/μm)
$\vec{F}, \vec{F}_{ext}$	external force on positive face of axoneme (pN)
$\vec{f}_{ij}$	force caused by link between ith and jth doublet (pN)
$\vec{\gamma}$	effective shear (radians)
$\vec{\kappa}$	curvature (rad/μm)
$\vec{L}_i$	vector from neutral axis to ith doublet (μm)
Λ	length of flagellum (μm)
$\vec{M}$	moment on positive face of axoneme cross section (pNμm)
$\vec{r}$	position vector (μm)
s	arc length (μm)
$\vec{S}$	internal shear force (pN)
$\vec{T}$	tangent vector
u_i	sliding of ith doublet relative to central pair (μm).

I. FLAGELLAR SHAPE

Consider an orthogonal coordinate system with its origin at arc length position s along the neutral axis (see Lubliner and Blum, 1971) of the axoneme. The location of this origin with respect to some fixed point in the laboratory is expressed by the position vector, $\vec{r}$. The orientation of this coordinate system is taken as fixed relative to the structure of the axoneme. We call this system the body coordinate system and, for convenience, choose to orient the z axis along the neutral axis of the axoneme, i.e., along the tangent. The orientation of the x axis can be arbitrarily fixed with respect to some conventional structural feature of the axoneme such as along the long cross section of the central pair. The y axis is then fixed by the further requirement that the body coordinate system be right-handed. The value of using such body coordinate systems is twofold. First, many mechanical and structural properties are independent of s when expressed in this system. Second, vectors describing structure, position, and forces acting on the axoneme have very simple representations. The shape of the axoneme can be envisioned as a continuous string of coordinate systems with their origins separated by an infinitesimal distance, ds, along the filament axis.

Fig. 1 illustrates how the overall shape is governed by the relative rotation of adjacent body coordinate systems. For example, pure twist is built up by successive relative rotations about the z axis and pure bending in the xz plane is built up by successive rotations about the y axis. The change of orientation with respect to arc length about the three local body coordinate axes are the three components of the curvature vector, κ_i, along these axes. Notice that we have identified κ_z as the amount of twist per unit arc length. As a flagellum changes its orientation continuously (but

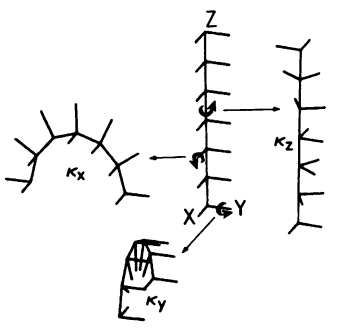

FIGURE 1 Bending and twist generated by relative rotation of adjacent body coordinate systems about the body coordinate axes. Rotation only about the z axis produces pure twist, κ_z. Rotation only about the x axis produces pure bending in the Y, Z plane, κ_x, and similarly about the y axis.

with $\kappa_z = 0$ everywhere) parts of the flagellum will rotate; such rotations should not be confused with twist. These concepts are rigorously expressed in the appendix where coordinate transformations are used to derive the usual expression for the directional derivative of a vector,

$$\frac{d\vec{V}}{ds} = \left(\frac{d\vec{V}}{ds}\right)_{body} + \vec{\kappa} \times \vec{V}. \tag{1}$$

This formula relates the change of a vector, $\vec{V}$, with respect to arc length, to the derivative of its components in the body coordinate system at position s; the cross product term accounts for possible changes in direction of the axes of the body coordinate system if the axoneme is undergoing bending or twisting. For example, because the tangent vector, T, has been defined so that it is constant in body coordinates,

$$\frac{d\vec{T}}{ds} = \vec{\kappa} \times \vec{T}. \tag{2}$$

Given $\vec{\kappa}(s)$ in body coordinates, one can determine the shape of the flagellum by using the transformation matrices described in the appendix. From Eq. A5, the infinitesimal transformation from position s to $s - ds$ is

$$\underset{\sim}{A}(s - ds, s) = \begin{bmatrix} 1 & -\kappa_z ds & \kappa_y ds \\ \kappa_z ds & 1 & -\kappa_x ds \\ -\kappa_y ds & \kappa_x ds & 1 \end{bmatrix}. \tag{3}$$

The finite transformation from position s back to the origin ($s = 0$) is then achieved by the infinite product of these infinitesimal transformations:

$$\underset{\sim}{A}(0, s) = \underset{\sim}{A}(0, ds)\underset{\sim}{A}(ds, 2ds) \ldots$$

$$\underset{\sim}{A}(s - 2ds, s - ds)\underset{\sim}{A}(s - ds, s). \tag{4}$$

Because $d\vec{r}/ds = \vec{T}$ in body coordinates is $\hat{z}$, then the position vector, $\vec{r}$, to the flagellum at position s from an origin at $s = 0$ is

$$\vec{r}(s) = \int_0^s \underset{\sim}{A}(0, s')\hat{z}ds'. \tag{5}$$

Thus in fixed coordinates the X, Y, and Z components of the position vector are

$$X(s) = \int_0^s A_{13}(0,s')ds'$$

$$Y(s) = \int_0^s A_{23}(0,s')ds'$$

$$Z(s) = \int_0^s A_{33}(0,s')ds'. \tag{6}$$

II. SLIDING FILAMENT MODEL

The position vector of the ith doublet of the axoneme can be written formally as

$$\vec{r}_i(s_i) = \vec{r}(s) + \vec{L}_i(s), \tag{7}$$

where $\vec{r}$ refers to the position vector of the central pair of microtubules (Fig. 2). The sliding filament model is expressed succinctly merely by requiring that $\vec{L}_i$, a vector from the central pair to the ith outer doublet, be a constant vector in body coordinates. We choose $\vec{L}_i$ normal to the central pair tangent vector. (For convenience $\vec{L}_i$ may be thought of as directed along an undistorted radial link.) This formalism then specifies that the normal distance between the central pair and any of the outer doublets is fixed, but allows the axoneme as a whole to bend and twist in three dimensions. It is important to realize that s_i in Eq. 7 is not an independent parameter, but is the arc length of the ith filament in the cross section of the axoneme at arc length s along the neutral axis. Warner's (1978) data shows that during extensive cross bridging the cilium assumes an ellipsoidal shape, i.e., is distorted, with some doublets approaching the central pair while others move some distance away. This refinement, which would require that the magnitude of L_i be a variable, is ignored here. It is implicit in this formulation that the central pair retains a fixed orientation relative to a marker (such as the position of the 5-6 bridge) somewhere on one of the outer doublets. If the central pair rotated within the interior of the cylindrical region defined by the outer doublets, as indicated by the studies of Omoto and Kung (1980), then the axonemal body coordinates in which $\vec{L}_i$ is constant could no longer be identified with central pair body coordinates. Although it would be simple to allow for rotation of the central pair relative to the outer cylinder of doublets, we ignore that possibility here.

The relationship between the tangent vectors of the central pair and the ith outer doublet can be obtained by differentiating Eq. 2.1 with respect to s,

$$\frac{d\vec{r}_i}{ds} = \frac{d\vec{r}}{ds} + \frac{d\vec{L}_i}{ds}. \tag{8}$$

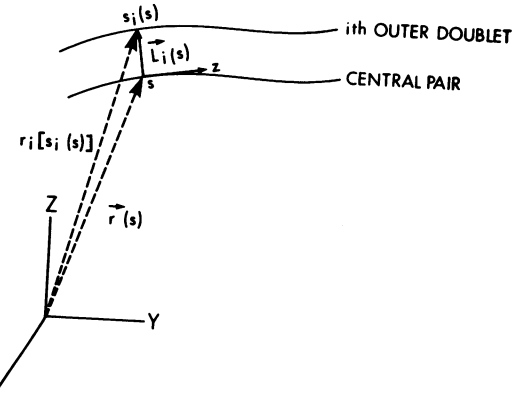

FIGURE 2 The central pair and the ith outer doublet of an axoneme are shown relative to a fixed coordinate system, XYZ. The body coordinate axis is tangent to the central pair (strictly, the neutral axis) at arc length position s, and $\vec{L}_i(s)$ is perpendicular to the tangent and has a fixed length.

The term on the left side of this equation is, by the chain rule, $(d\vec{r}_i/ds_i)\,(ds_i/ds)$. Because $\vec{L}_i$ is a constant in body coordinates, $d\vec{L}_i/ds = \vec{\kappa}(s) \times \vec{L}_i(S)$. Thus Eq. 8 can be rewritten as

$$\frac{ds_i}{ds}\vec{T}_i = \vec{T}(s) + \vec{\kappa}(s) \times \vec{L}_i(s), \tag{9}$$

where we have used the fact that the arc length derivative of the position vector is the tangent vector. If one defines the relative sliding, $u_i(s)$, as $s - s_i(s)$ (note that positive sliding or distal movement makes the value of $s_i < s$), then upon taking the norm of Eq. 9 one obtains

$$\frac{du_i(s)}{ds} = 1 - |\vec{T}(s) + \vec{\kappa}(s) \times \vec{L}_i(s)|. \tag{10}$$

If the twist per unit arc length, κ_z, is not too great, the norm in Eq. 10 can be expanded in a Taylor's series to yield the second-order approximation,

$$\frac{du_i}{ds} = -(\vec{L} \times \vec{T}) \cdot \vec{\kappa} - (L_i\kappa_z)^2/2. \tag{11}$$

This equation is exact if $\kappa_z = 0$ (i.e., no twist). Notice also that $\vec{L} \times \vec{T}$ has no z component; thus, to first order, sliding is independent of twist.

For planar bending without twist the integral of Eq. 10 equals L times the total bend angle. For pure twist ($\kappa_x = \kappa_y = 0$) sliding of the outer doublets relative to the central pair occurs because of the increased length of the spiral path. Fig. 3 demonstrates the accumulation of sliding at the tip for a three-filament axoneme (outer filaments numbered 1 and 2) with constant κ_z and constant κ_x and, for convenience, $\kappa_y = 0$. In the linear approximation, $u_2 - u_1$ is $2\kappa_x L\Lambda$ at the distal end, where Λ is the length of the axoneme. In the second-order approximation, $u_1 = (-\kappa_x L - 0.5L^2\kappa_z^2)\Lambda$ and $u_2 = (\kappa_x L - 0.5L^2\kappa_z^2)\Lambda$, and again

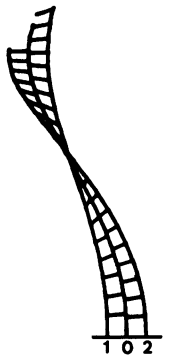

FIGURE 3 A three-filament axoneme with the central filament labeled 0 and two outer doublets labeled 1 and 2 is shown. The filaments, fixed at the base, are 20 μm long and the spacing between the central filament and filaments 1 and 2 is +1 and −1 μm, respectively, in the body coordinate x axis. Curvature is set at $\kappa_x = 4.5$, $\kappa_y = 0$, $\kappa_z = 9$ degrees/μm. Markers spaced at 1 μm intervals along the outer doublets and normal to them as well as to the central pair are shown as an aid to visualizing the twist and the sliding.

$u_2 - u_1$ is $2\kappa_x L\Lambda$. The exact relative sliding (from Eq. 10), however, is

$$u_2 - u_1 = [\sqrt{(1 + \kappa_x L)^2 + \kappa_z^2 L^2} - \sqrt{(1 - \kappa_x L)^2 + \kappa_z^2 L^2}]\Lambda\,. \tag{12}$$

The exact value for $u_2 - u_1$ therefore contains a very small (order $\kappa^3 L^3$) contribution due to twist. For a flagellum 20 μm long with a spacing of 0.1 μm between central pair and an outer doublet, a κ_x of 4.5 degrees/μm and a κ_z of 9.0 degrees/μm, the value of $u_2 - u_1 = 0.315789$ μm to second order, and the exact result is 0.315790.

Schreiner (1977) has derived equations that allow one to compute the displacement and sliding of twisted filaments in cilia and flagella, and Holwill et al. (1979) modified the treatment of Schreiner (1977) for ease of computation of the doublet pattern to be expected at the tip of cilia in the effective and recovery stroke positions. Their derivation accounts for the changing projection of the filaments onto the plane of bending, but ignores the sliding due to spiraling of the filaments about the central pair. If, for example, the twist was so large that the doublets essentially coiled around the base of the flagellum, their equations would predict zero sliding relative to the central pair, whereas the actual sliding would be almost the negative of the full length of the flagellum. Although the equations used by Holwill et al. (1979) are correct only to first order, their use to compute relative sliding of outer doublets eliminates terms equivalent to the term $(L\kappa_z)^2/2$ in Eq. 11, so that their computations of relative tip displacements are correct to second order and hence entirely adequate.

III. BENDING RESISTANCE OF THE AXONEME

By bending resistance we mean the sum of the bending resistance of the individual doublets. Other contributions to "stiffness" from interdoublet links such as nexin links, radial spokes, or dynein cross-bridges, will be treated as contributing to shear resistance. Even if one assumes that the bending resistance of individual doublets is linearly elastic (i.e., the bending moment is proportional to curvature), it is not clear whether the axoneme can be treated so simply. For example, in a twisted but otherwise straight axoneme, the outer doublets would spiral around the central pair and their direction would not be parallel to the axonemal axis. Axonemal bending resistance might thus be a complicated function of shape. In this section we examine this question and ask under what conditions it is appropriate to use a simple linear elastic bending resistance to describe the bending resistance of a flagellum.

The assumption that individual doublets are linearly elastic can be expressed as

$$\vec{M}_i = -\underset{\sim}{E}_{bi}\vec{\kappa}_i. \tag{13}$$

Here $\vec{M}_i$ is the bending moment and $\underset{\sim}{E}_{bi}$ is the bending resistance of the ith filament. The representation of bend-

ing resistance in ith doublet body coordinates is particularly simple; because we have chosen the coordinate axes to lie along the principal axes of the doublet, all off-diagonal terms of the matrix are zero, and

$$\underset{\sim}{E}_{bi} = \begin{bmatrix} E_{xx} & 0 & 0 \\ 0 & E_{yy} & 0 \\ 0 & 0 & E_{zz} \end{bmatrix}. \tag{14}$$

To derive reasonable values for the components of the bend resistance matrix, we make use of a generalized form of Hooke's law, which states that linear strain is proportional to force per unit area via $\epsilon_x = [\sigma_y - \nu(\sigma_y + \sigma_z)]/E$, with similar equations for the y and z components of the strain, ϵ. In this equation, σ_y and σ_z are the forces acting per unit area on the y and z faces of an infinitesimal element of the body, E is Young's modulus of elasticity, and ν is Poisson's ratio,[1] a number that ranges from $\simeq$0.3 for metals to $\simeq$0.5 for rubber. Hooke's law also states that the shear force is proportional to the shear strain via the shear modulus $G = E/2(1 + \nu)$. It can be shown (Crandall and Dahl, 1959) for slender members that the twisting moment generated by κ_z is given by

$$M_z = -GI_{zz}\kappa_z, \tag{15}$$

where I_{zz}, is the moment of inertia around the Z axis. Similarly, the bending moment is given by

$$M_i = -EI_{ij}\kappa_j \; i = 1, 2 \tag{16}$$

where $I_{ij} = \int_A x_i x_j dA$. Electron microscopic studies show that typical dimensions for an outer doublet are ~20 nm from the center of the B subfiber to the center of the A subfiber, and wall thickness is ~5 nm. For convenience of computation, we replace the outer doublet by a pair of overlapping tubules, as shown in Fig. 4. The area of one of the annuli is $2\pi|r'|t$. The moments of inertia are given by

$$I_{zz} = 2\int_A r^2 dA = 2\int_A (x_o + r')^2 dA = 2 \text{ Area } (X_o^2 + r'^2),$$

$$I_{xx} = 2\int_A (X_o + r'\cos\theta)^2 r t d\theta = 2 \text{ Area } \left(X_o^2 + \frac{r'^2}{2}\right),$$

and

$$I_{yy} = 2 \text{ Area } \frac{r'^2}{2}. \tag{17}$$

Using a value of $E = 4 \cdot 10^7$ pN/μm^2 (Hines and Blum, 1979) and choosing $\nu = 1/3$, one obtains the following approximate values for the bend resistances of an individual doublet: $E_{xx} = 3.6$, $E_{yy} = 1.2$, $E_{zz} = 5.4$ p$N\,\mu$m^2. Recent measurements of the bending resistance of isolated doublets (Ishijima and Hiramoto, 1982, and personal communication), however, indicate a value for bend resistance of ~10 p$N\,\mu$m^2, suggesting that the above value of E may be too low for a tubulin doublet.

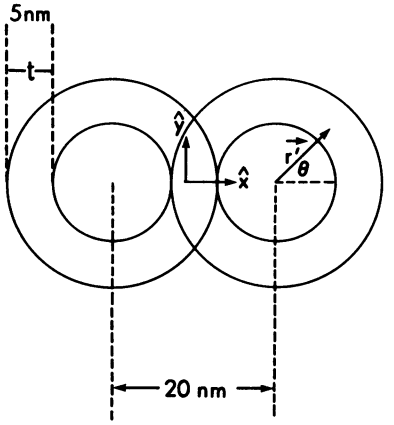

FIGURE 4 Shape used for computation of moment of inertia of an outer doublet. For simplicity of computation, a doublet is drawn as two overlapping singlets with the dimensions shown. This slightly overestimates the moment of inertia in the overlap region, but this is more than compensated for by use of the average value of the radius of the annulus in the computation of the moment of inertia. Because the body coordinates are oriented as shown (with the x axis perpendicular to the paper), the off-diagonal elements of the moment of inertia matrix are zero by symmetry. $\vec{X}_o$ (not shown) is a vector from the origin of the coordinate system to the center of either singlet microtubule.

The bending moment of the axoneme is just the sum of the bending moments of the individual filaments. To find $\underset{\sim}{E}_b$, we choose a curvature for the central pair, find the curvature for each of the outer doublet filaments (using Eq. 9, appropriate to a sliding filament model with no distortion of the axoneme), then use Eq. 13 to find the moments of each filament, and add those moments together. We then do the same thing for slightly different curvatures of the central pair to build an expression for E_b, via $E_{b_{ij}} = \delta M_i/\delta\kappa_j$.

To carry out this program, it is first necessary to find a transformation matrix, which we denote $\underset{\sim}{A}_{io}$, from central pair body coordinates to ith outer doublet body coordinates. Once the vectors of interest (i.e., bending moment vectors) are expressed in the same coordinate system, conventional vectorial operations can be done component by component.

$\underset{\sim}{A}_{io}(s)$, the transformation from central pair body coordinates to the ith outer doublet body coordinates at arc length $s_i(s)$ is simply the product of three elementary rotations, $\underset{\sim}{A}_{io} = \underset{\sim}{B}\underset{\sim}{C}\underset{\sim}{D}$. The first of these, $\underset{\sim}{D}$, is a rotation about the central pair z axis by an amount θ, so that the new x' axis is along $\vec{L}_i$ (Fig. 5):

$$\underset{\sim}{D} = \begin{bmatrix} \cos\theta_i & \sin\theta_i & 0 \\ -\sin\theta_i & \cos\theta_i & 0 \\ 0 & 0 & 1 \end{bmatrix}. \tag{18}$$

[1]When an elastic material is stretched, it also becomes slightly thinner. If the initial length and diameters are l_o and d_o, respectively, then ν = − lateral strain/longitudinal strain = $-[(d - d_o)/d_o]/[(l - l_o)/l_o]$.

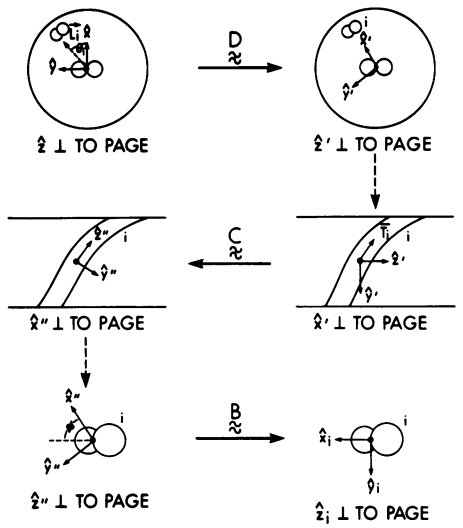

FIGURE 5 Shown are three elementary coordinate transformations used to build up the finite transformation from central pair body coordinate to ith doublet. The solid horizontal arrows between similar views imply a transformation of coordinates. The dashed vertical arrows between different views denote merely a change in the observer's viewpoint to allow easy visualization of the following transformation.

Next, we rotate about the x' axis by the amount required for the new z'' axis to be in the direction $\vec{T}_i$. To find the transformation, $\underset{\sim}{C}$, we use two pieces of information. First, the representation of $\vec{L}_i$ in double prime coordinates is the same as it is in prime coordinates, as we are rotating about an axis parallel to $\vec{L}_i$. Thus

$$\begin{pmatrix} L \\ 0 \\ 0 \end{pmatrix} = \underset{\sim}{C} \begin{pmatrix} L \\ 0 \\ 0 \end{pmatrix}. \tag{19}$$

The second piece of information is that $\vec{T}_i = \hat{z}''$. From Eq. 9, the representation of $\vec{T}_i$ in prime coordinates is

$$T_i' = \frac{\begin{pmatrix} 0 \\ 0 \\ 1 \end{pmatrix} + \begin{pmatrix} \kappa_{x'} \\ \kappa_{y'} \\ \kappa_{z'} \end{pmatrix} \times \begin{pmatrix} L \\ 0 \\ 0 \end{pmatrix}}{\frac{ds_i}{ds}}. \tag{20}$$

Eq. 19 and 20 imply that

$$\underset{\sim}{C} = \begin{bmatrix} 1 & 0 & 0 \\ 0 & \dfrac{1 - L\kappa_{y'}}{ds_i/ds} & \dfrac{L\kappa_{z'}}{ds_i/ds} \\ 0 & \dfrac{L\kappa_{z'}}{ds_i/ds} & \dfrac{1 - L\kappa_{y'}}{ds_i/ds} \end{bmatrix} \tag{21}$$

with

$$ds_i/ds = [(L\kappa_{z'})^2 + (1 - L\kappa_{y'})^2]^{0.5}. \tag{22}$$

The matrix $\underset{\sim}{B}$ is the transformation for a rotation about z'' by an angle ϕ and therefore has the same form as that of matrix $\underset{\sim}{D}$ (see Eq. 18). Notice that because of matrix $\underset{\sim}{C}$, $\underset{\sim}{A}_{io}$ is a function of curvature. The bending moment of the axoneme as a whole can then be written as follows,

$$\vec{M}_{\text{axoneme}} = -\left[\underset{\sim}{E}_{bo} + \sum_{i=1}^{9} \frac{1}{ds_i/ds} (\underset{\sim}{A}_{io}^{-1} \underset{\sim}{E}_{bi} \underset{\sim}{A}_{io})\right] \vec{\kappa}. \tag{23}$$

The first term in this equation is the bending moment of the central pair. In the second term, ds_i/ds accounts for the fact that for a given change in bend angle there are different arc lengths for each outer doublet and hence different curvatures. This is usually ignored in treatments of planar motion, but differs from unity whenever curvature is large or when there is appreciable twist. The term in parentheses represents the ith outer doublet bending resistance in central pair body coordinates, and also depends on curvature.

For a straight flagellum using the bend resistance values derived above, the values of E_{xx}, E_{yy}, and E_{zz} for the whole axoneme are 25.2, 22.8, and 54.0 pN μm^2, with the off-diagonal elements $<10^{-6}$ pN μm^2. Thus the effect of averaging the contribution of the doublets with that of the central pair is to produce a bend resistance matrix which is only slightly acylindrical ($E_{xx} \simeq E_{yy}$). Furthermore, the magnitudes of bend resistance are identical to the average contribution of the outer doublets plus 3.6 or 1.2 due to the central pair. The twist resistance, on the other hand, is simply the sum of the individual twist resistances of each doublet. For a helical flagellum with $\kappa_x = \kappa_y = \kappa_z = 1$ rad/μm, the bending moment computed from Eq. 23 has components $M_x = 25.8$, $M_y = 23.4$, and $M_z = 54.5$ pN μm. If the bending resistance of the straight axoneme were applicable to a flagellum with this curvature, the bending moment components (using the same form as Eq. 3.1) would be $M_x = 25.2$, $M_y = 22.8$, and $M_z = 54.0$ pN μm. Thus, even with this very large degree of curvature, a <5% error is made in the bending moment if one uses a constant E_b. It is interesting to note that the bend resistance matrix with this curvature has diagonal elements 26.0, 23.6, and 53.3 pN μm^2 (instead of 25.2, 22.8, and 54.0 pN μm^2 for the straight flagellum), and the off-diagonal terms range from 0.2 to 1.2 pN μm^2 (instead of $<10^{-6}$ pN μm^2). Clearly it is an excellent approximation to consider E_b as being independent of curvature. In the simulations to be presented below, we will use E_b appropriate for a straight axoneme, which is applicable with negligible error to normally curved flagella and cilia.

IV. SHEAR MOMENTS

The only components of force between filaments that are of interest are those that tend to move any of the doublets in ways that are allowed. Thus forces that tend to distort the axoneme by, e.g., moving an outer doublet closer to or farther from the central pair are ignored, because we

assume that forces of constraint exist that prevent such motion (i.e., that exactly balance the forces tending to produce such distortion). All components of forces along the direction of any of the doublets, however, must be accounted for, because they will produce relative sliding. Thus, in so far as the radial link system merely acts to prevent axonemal distortion, it will not contribute to sliding. If the radial link system, however, undergoes a cyclic attachment-detachment process and resists relative sliding while attached, its contributions to the production of bending moments cannot be ignored. Until further information is available as to the details of operation of the radial link system, we shall assume that it acts only to prevent distortion and as a source of passive shear resistance. The treatment that we now develop for the peripheral nexin links can, however, be easily extended to include the contribution of the radial link system to sliding when a detailed model of its action is proposed.

Link forces contribute to the tension in the outer doublets, and these tensions, because they are a distance L_i from the body coordinate z axis, have resultant moments. Fig. 6 illustrates how the moment proximal to a stretched link is computed for links that cannot themselves transmit moments, i.e., pinned links. We write the tension in the ith filament at arc length s_i, where it passes through the cross section at arc length s, as

$$\text{Tension}_i = \sum_{j \to i} \vec{T}_i(s) \int_{s_i}^{\Lambda}(s)\, \vec{T}_i(s') \cdot \vec{f}_{ij}(s')\mathrm{d}s', \qquad (24)$$

where we have approximated the links between the ith and jth filaments as a continuous distribution and the sum is over all filaments that have links connecting to the ith filament. For nexin links there are only two terms in this sum because the ith outer doublet ($i = 1 \ldots 9$) has nexin links only with the two adjacent doublets. For radial links, there would be one term for each outer doublet and nine terms for the central pair. The total moment due to these links is then

$$\vec{M}(s) = \sum_{i=1}^{9} \sum_{j \to i} \{\vec{L}_i(s) \times \vec{T}_i(s) \int_{s_i(s)}^{\Lambda} [\vec{T}_i(s') \cdot \vec{f}_{ij}(s')]\mathrm{d}s'\}. \qquad (25)$$

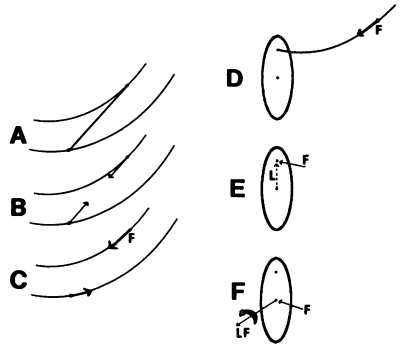

FIGURE 6 The conceptual process involved in determining the bending moment at some point proximal to a stretched link. In panels A–C, the stretched link produces a force along the link but constraints (not shown) keeping the filaments a constant distance apart exactly balance the force components that are not tangent to the filament. In panel D, the force $\vec{F}$ of panel C produces a constant tension along the filament proximal to the link. In panels E and F, the tension in the filament is a distance L from the origin of the cross section, thus producing a moment of magnitude LF as well as a tension F along the axonemal axis.

In the usual first-order approximation it is appropriate to assume that (a) $s_i(s) = s$, i.e., that opposite ends of a link are not located at significantly different arc length; (b) $\vec{T}_i(s) = \vec{T}(s)$, i.e., that the doublets at opposite ends of a link have similar tangents. This approximation implies that

$$-\frac{\mathrm{d}\vec{M}}{\mathrm{d}s} = \vec{S} = \sum_{i=1} \sum_{j \to i} \vec{L}_i \times \vec{T}(\vec{T} \cdot \vec{f}_{ij}), \qquad (26)$$

i.e., that the links produce only a shear force, $\vec{S}$, to first order. It is of interest, however, to ask if the twisting moment generated by the action of links in a sliding filament system is significant. To assess the magnitude of the twisting moment, we retain the first-order term in the approximation to $\vec{T}_i$, i.e., $\vec{T}_i = \vec{T} - \kappa_z(\vec{L} \times \vec{T})$ (see Eq. 9).

The twisting moment, $\vec{M}_z$, from Eq. 25 is then given by

$$\vec{M}_z = \sum_{i=1} \sum_{j \to i} \kappa_z L_i^2 \int_s^{\Lambda} (\vec{T} \cdot \vec{f}_{ij}) ds'. \qquad (27)$$

For elastic peripheral links (i.e., nexin links), $\vec{M}_z = 0$ as $f_{ij} = -f_{ji}$ and L_i is a constant. Thus any twisting moment due to peripheral links is at least third order in L_i and hence negligible. For radial links, the first summation should go from $i = 0$ to $i = 9$, where $i = 0$ represents the central pair. The forces, $\vec{f}_{io}$, exerted on the ith outer doublet contribute a twisting moment, but $-\vec{f}_{oi}$ (acting on the central pair) do not contribute a twisting moment. Thus radial links contribute a (second order in L_i) twisting moment, proportional to the twist component of curvature, κ_z. The twisting resistance due to the elasticity of the filaments is E_{zz}. The twisting resistance of the axoneme due to radial links is

$$\sum_{i=1}^{9} L_i^2 \int_s^{\Lambda} (\vec{T} \cdot \vec{f}_{io})\, \mathrm{d}s'. \qquad (28)$$

Before attempting to assess the magnitude of this twisting resistance term, it is convenient to return to the shear force (Eq. 26) and cast it in a form suitable for analysis. We begin by assuming that the doublets are firmly tied together at the proximal end, i.e., $u_i(0) = 0$ for $i = 0 \ldots 9$. If we ignore the second-order effect of twist on sliding in Eq. 11 it becomes

$$\frac{\mathrm{d}u_i}{\mathrm{d}s} = -\vec{\kappa} \cdot (\vec{L}_i \times \vec{T}). \qquad (29)$$

The effective shear, $\vec{\gamma}$, analogous to the definition of γ used for the analysis of planar motion (Hines and Blum, 1978) can now be written as

$$u_i = -\vec{\gamma} \cdot (\vec{L}_i \times \vec{T}) \qquad (30)$$

thereby allowing one to use $\vec{\gamma}$ instead of the nine values of u_i. Because both $\vec{L}_i$ and $\vec{T}$ are constant in body coordinates, Eqs. 29 and 30 are consistent if the three body coordinate components ($k = 1, 2, 3$) are defined by the relation $d\gamma_k/ds = \kappa_k$. Because $u_i(0) = 0$, $\vec{\gamma}(0) = 0$ and when twisting is small, plane sections will remain planar in three-dimensional bends. Under these conditions, and in so far as the radial links can be treated as a passive system, the twisting resistance of the axoneme due to the radial links will be zero to second order because the tension, $\int_s^\Lambda (\vec{T} \cdot \vec{f}_{io})ds'$, on opposite sides of the axoneme will cancel. The contribution of an active radial link system to twist resistance could only be evaluated in terms of a specific model for the behavior of the radial links. If the constraints on axonemal distortion were relaxed so that the central pair was free to rotate it is easy to envision how an active radial link system could cause rotation of the central pair.

For further evaluation of the shear force we assume that a nexin link produces a linear elastic force proportional to its length and that the radial links act merely as structural constraints. Then

$$\vec{f}_{ij} = -E_s^*(u_{ij}\vec{T} + \vec{L}_{ij}), \tag{31}$$

where now i and j denote adjacent doublets with relative sliding $u_{ij} = u_i - u_j$ and separation $\vec{L}_{ij} = \vec{L}_i - \vec{L}_j$ and E_s^* is the resistance of a nexin link to stretch.

To get the contribution of the nine nexin links within an axonemal cross section at s to the shear force at s^* we treat the sum in Eq. 26 as an integral,

$$\vec{S} = \frac{9}{2\pi}\int_0^{2\pi} (\vec{L}_{ij} \times \vec{T})(\vec{T} \cdot \vec{f}_{ij})d\theta \tag{32}$$

with $\vec{f}_{ij}$ specified in Eq. 31 and $\vec{L}_{ij}$ represented in body coordinates by

$$\vec{L}_{ij} = L\left\{\left[\cos\theta - \cos\left(\theta - \frac{2\pi}{9}\right)\right]\hat{x} + \left[\sin\theta - \sin\left(\theta - \frac{2\pi}{9}\right)\right]\hat{y}\right\}. \tag{33}$$

After some algebraic manipulation, one finds

$$\vec{S}_{nexin} = -\frac{d\vec{M}_{shear}}{ds} = -E_s(\gamma_x\hat{x} + \gamma_y\hat{y}). \tag{34}$$

where $E_s = 2\pi^2/9\, L^2 E_s^*$.

As noted above, the present analysis has been confined to pinned links, i.e., links that cannot support a moment at their point of attachment. Because attached dynein arms are unlikely to behave as pinned links, it is possible that the action of dynein arms could generate twist. An analysis of the capacity of dynein arms to generate twist will require an extension of the present formalism. The present analysis, therefore, is merely the first step in understanding the factors contributing to twist generation in cilia and flagella.

V. COMPUTATIONS FOR STATIC EQUILIBRIA

Equilibrium Equations

In sections III and IV we have derived expressions for the bending moments due to the bending and shear resistances of the axonemal components. At equilibrium the sum of all of the bending moments, $\vec{M}_b + \vec{M}_s + \vec{M}_{ext}$, must vanish at every point on the flagellum, where $\vec{M}_b$ is the moment due to axonemal bending resistance, $\vec{M}_s$ is the moment arising from all internal shear producing or resisting links, and $\vec{M}_{ext}$ is the moment due to external forces such as viscosity. In this paper we treat only static equilibrium, where the viscous moment is zero. For purposes of numerical computation the most convenient way to express the equilibrium condition is in terms of the three component derivatives of the moment balance equation, expressed in body coordinates. From Eqs. 13 and 14,

$$-E_{bij}\frac{d^2\gamma_j}{ds^2} - S_i + \frac{dM_{ext_i}}{ds} = 0. \tag{35}$$

We have shown earlier (Blum and Hines, 1979) that an external force per unit length, $\vec{\phi}$, produces an external moment through the equations

$$\frac{d\vec{F}_{ext}}{ds} + \vec{\phi} = 0, \tag{36}$$

and

$$\frac{d\vec{M}_{ext}}{ds} + \vec{T} \times \vec{F}_{ext} = 0, \tag{37}$$

where $\vec{F}_{ext}(s)$ is the force on the positive face of a cross section of flagellum due to all external forces proximal to that cross section. Eqs. 35–37 determine the shape of a flagellum given an external force and appropriate boundary conditions. At the distal end ($s = \Lambda$), $\vec{M}_{ext} = \vec{M}_s = 0$, and therefore $\vec{M}_b = 0$. Thus $d\gamma_j(\Lambda)/ds = 0$ for the body coordinates $j = 1, 2, 3$. The application of a point force at the distal end implies that $\vec{F}_{ext}(\Lambda) = \vec{\phi}(\Lambda)ds$. If the applied force were distributed over a region of the axoneme, as would be the case for viscous forces, then $\vec{F}_{ext}(\Lambda) = 0$ because ds is infinitesimal. If the external force were applied at the tip as, for instance, a needle point, then $\vec{\phi}(\Lambda)$ would be a delta function such that $\vec{\phi}(\Lambda)\, ds$ equals the total force applied by the needle. A further boundary condition is the constraint that there is no sliding at the proximal end, i.e., $\gamma_j(0) = 0$. This implies that $S_j(0)$ takes on whatever shear force is necessary to prevent sliding at $s = 0$. The final boundary condition depends on whether the proximal end is free, in which case the proximal force and moment are equal to zero, or embedded in a wall, in which case we know the proximal position and angle with respect to fixed coordinates. In this paper we deal only with the latter case.

In the absence of an external force, $\vec{\mathbf{M}}_{ext}(s) = 0$. Because $\vec{\mathbf{S}}$ has no tangential component, $S_3 = 0$. Then from Eq. 5.1, $E_{b_{jj}} d^2\gamma_j/ds^2 = 0$. Because the tangential direction of a cylinder is necessarily one of the principal axes of the bend resistance matrix, $d^2\gamma_3/ds^2 = 0$. Thus shear forces, whether produced by peripheral links or passive radial links cannot produce twist. In the absence of external forces and of moment transmitting links, the problem of three-dimensional motion can be reduced to that of two independent planar problems.

Computational Methods

Eqs. 35–37 with associated boundary conditions may be solved numerically by defining $\vec{\gamma}(s)$ and $\vec{\mathbf{F}}_{ext}(s)$ in body coordinates at $N + 1$ points, $p = 0 \ldots N$, separated by distance Δs, with $p = 0$ and $p = N$ defining the proximal and distal ends, respectively. $\vec{\mathbf{M}}_{ext}(s)$, $\vec{\kappa}(s)$, and $\vec{\phi}(s)$ (in body coordinates) are defined at the N intermediate points, e.g., $\vec{\mathbf{M}}[(p + 0.5)\,\Delta s]$. Eqs. 35 and 37 are evaluated at points p and Eq. 36 is evaluated at points $(p + 0.5)$ using approximations correct to order Δs^2. Thus the equations for coordinates $i = 1, 2, 3$ are written,

$$-(E_{bij}/\Delta s^2)[\gamma_j(p+1) - 2\gamma_j(p) + \gamma_j(p-1)] - S_i(p) + (1/\Delta s)[M_i(p+0.5) - M_i(p-0.5)] = 0, \quad p = 1 \ldots N-1 \quad (38)$$

$$(1/\Delta s)[F_i(p+1) - F_i(p)] + \left\{\frac{[\vec{\gamma}(p+1) - \vec{\gamma}(p)]}{\Delta s} \times \frac{[\vec{\mathbf{F}}(p+1) + \vec{\mathbf{F}}(p)]}{2}\right\}_i + \vec{\phi}_i(p+0.5) = 0, \quad p = 0 \ldots N-1 \quad (39)$$

and

$$(1/\Delta s)[M_i(p+0.5) - M_i(p-0.5)] + \left\{\frac{\gamma(p+1) - \gamma(p-1)]}{2\Delta s} \times \frac{(\vec{\mathbf{M}}(p+0.5) + \vec{M}(p-0.5)]}{2}\right\}_i + [\vec{\mathbf{T}} \times \vec{\mathbf{F}}(p)]_i = 0, \quad p = 1 \ldots N-1. \quad (40)$$

In these equations, the cross product terms come about because Eqs. 36 and 37 contain vector derivatives (see Eq. 1). The boundary conditions are expressed as

$$\gamma_i(0) = 0, \quad (41)$$

$$\vec{\mathbf{M}}_i(N - 0.5) = -F_i(N)\Delta s/2, \text{ and} \quad (42)$$

$$\gamma_i(N) - \gamma_i(N-1) = 0. \quad (43)$$

Note that for simplicity Eq. 43 is correct only to first order. Because S_i in Eq. 38 and the cross product terms in Eqs. 39 and 40 are nonlinear, this set of equations must be solved by an iterative procedure. At the kth iterative step the linear variation of each nonlinear term, say W_s, with respect to the variable x, is computed numerically as

$$W(x^k) = W(x^{k-1}) + [W(x^{k-1} + h) - W(x^{k-1})]\,(x^k - x^{k-1})/h \quad (44)$$

where h is a small number. The resulting linear equations are solved by Gaussian elimination. The iterations are performed until the difference between the values of the sum of the variable differences between the kth and $k - 1$th iterations is $<10^{-4}$.

Effect of Asymmetrical Bend Resistance on Twist

In the absence of internal shear forces, twisting may arise if an external force that is not along either the thick or the thin axis of the central pair is applied to an initially straight flagellum. Fig. 7 (left panel) illustrates this for a normal force applied at the distal end to bend the flagellum by 90°. The amount of twist depends on the plane of the bend relative to the central pair, the magnitude of the twist resistance, and the ratio of the thick and thin axis bending resistances. As shown in the right-hand panel, the amount of twist is small even for a thick-to-thin axis bend-resistance ratio of 2, i.e., 50 vs. 25 pN μm^2. For a real flagellum the ratio between thick and thin axis bending resistances is close to unity (see section III) so that application of an external force in the absence of shear resistance would not cause appreciable twist. For a given ratio (say 50 vs. 25 pN μm^2) the amount of twist is not directly proportional to the twist resistance (cf. the dotted line, with $E_{xx} = 25$, $E_{yy} = 50$, $E_{zz} = 25$ with the solid line labeled 50, for which $E_{xx} = 25$, $E_{yy} = 50$, and $E_{zz} = 54$ pN μm^2). When E_{yy} equals 200 pN μm^2 (with $E_{xx} = 25$ and $E_{zz} = 54$ pN μm^2), the shape of the flagellum becomes complex so that the plot of total twist vs. angle from the y axis is of little interest and is therefore not plotted. It should be noted that the equilibrium shape in these simulations was independent of the previous computational history.

Effect of Asymmetrical Shear Resistance on Twisting

The simulations in this section were carried out for a cylindrical bend resistance matrix ($E_{xx} = 300$, $E_{yy} = 300$, $E_{zz} = 500$ pN μm^2) but with different shear resistances along the x and y body coordinate axes. The presence of an asymmetrical shear resistance causes the equilibrium shape to depend on computational history. In Fig. 8, the force is applied initially along the fixed x direction with the magnitude required to bend the distal end by 45° with respect to the fixed x axes, and then that force is rotated in steps of 5° with magnitude adjusted to keep the distal end at 45° to the z axis so that at the end of the series of steps the force is 60° with respect to the x axis. In Fig. 9, the

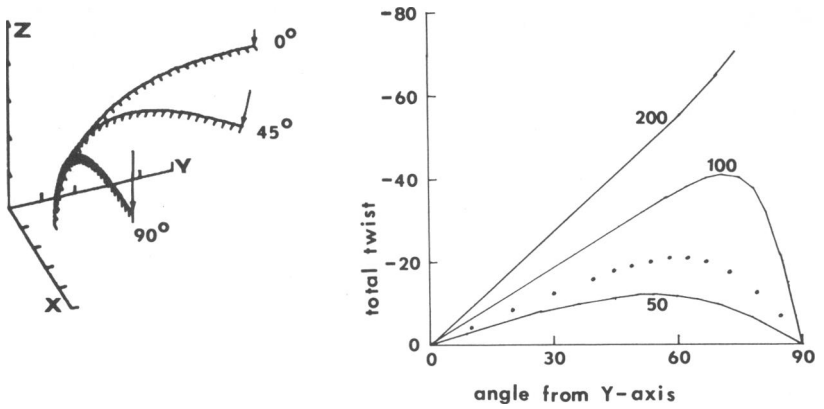

FIGURE 7 Twist due to an external force and an asymmetric bending resistance. A filament is bent by the action of an external force (left panel, arrows) so that the tangent at the distal end is normal to the fixed Z-axis. The external force applied at the distal end is at all times normal to the tangent. Bending resistances of the thin and thick axes were 25 and 100 pN μm^2, respectively, and twisting resistance was 54 pN μm^2. The direction and relative magnitude of normal force which caused the distal end tangent to be 0°, 45°, and 90° from the fixed Y-axis and normal to the Z-axis are shown as arrows. At 0° and 90° the external force is in the negative Z direction. It takes four times the force to bend the filament along the thick axis and there is no twist. At 45° the external force is not in the Z direction and the twist is 28°. The right-hand panel shows total twist at the distal end as a function of the angle of the distal end-tangent from the Y-axis for thick axis bending resistances of 50, 100, and 200 pN μm^2. The 200 pN μm^2 filament displays very complex behavior at large angles and only the linear portion is plotted. The dotted line is for thick axis bending and twisting resistances of 100 pN μm^2 each.

force was first applied in the fixed y direction and then rotated in steps of $-5°$, keeping the distal end 45° from the z axis, such that in the final equilibrium the force is 60° from the x axis. The two left panels of each of these figures show two views of the final equilibrium position. Comparison of Fig. 8 with Fig. 9 shows that the final shapes differ. The components of the curvature vector are also displayed in each figure. It can be seen that in the presence of asymmetric shear resistance the final shape depends on the previous computational history. We have not attempted to ascertain the maximum ratio of E_{sx} to E_{sy} for which final shape is independent of history. (This ratio would probably depend on E_b.) It is noteworthy that in both simulations an oscillation in the sign of the curvature components occurs and that the wavelengths are comparable. We also note that had the proximal end of the flagellum been free to rotate, then the final configuration would lie in a plane and shape would be independent of previous history.

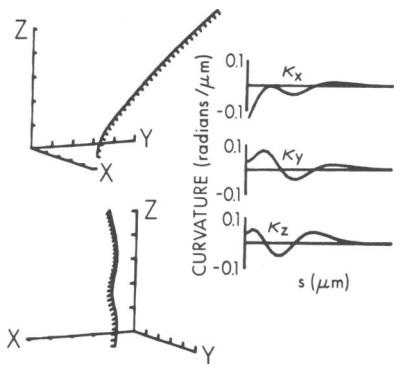

FIGURE 8 An axoneme 40 μm long is anchored in the XY plane at X = 10 μm, Y = 10 μm, Z = 0. The filaments are assumed to be tied at the proximal end. A point force parallel to the XY plane was applied at the distal end initially in the X direction until the distal end was 45° with respect to the Z axis. The force required to achieve this configuration was 11.8 pN. The direction of this point force was then rotated to the XY plane in steps of 5° and adjusted in magnitude so that the tangent at the distal end was maintained at 45° with respect to the Z axis until the final force (of magnitude 11.1 pN) was at 60° with respect to the X axis. The two left panels of this figure show two views of the flagellum in its final configuration. At the distal end, the twist was 23.3°, the direction of the tangent to the X axis was 48°, and the sliding components were γ_x = 0.44 rad and γ_y = 0.51 rad. The components of the curvature vector, $\vec{\kappa}$, are shown as a function of arc length in the right-hand side of the figure. Parameter values used in this simulation were, for the bending resistances, E_{xx} = 300, E_{yy} = 300, E_{zz} = 500 pNμm^2, for the shear resistances, E_{sx} = 10, E_{sy} = 8 pN.

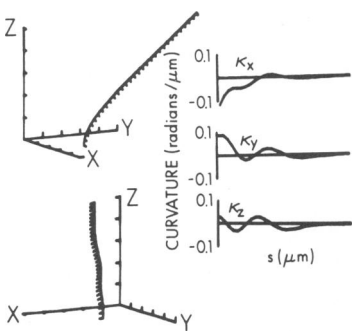

FIGURE 9 This simulation is identical to that shown in Fig. 8 except that the sequence of forces that brought it to the final configuration shown in the left panels began with a force of magnitude 14.8 pN directed along the y axis, followed by rotations of $-5°$ until the force was 60° from the X axis. The magnitude of the final force was 13.3 pN. At the distal end the twist was $-10.6°$, the direction of the tangent to the X axis was 61.7° (and to the Z axis was 45°), and the sliding components were γ_x = 0.64 rad and γ_y = 0.37 rad.

DISCUSSION

Crowley et al. (1981) have considered the propagation of three-dimensional bends along an axoneme in terms of two orthogonal noncoupled, planar, bending-moment equilibrium equations. The present paper shows that such a formulation is satisfactory for shear forces caused by pinned links even if the bending resistance is not radially uniform. The present work also permits the computation of twisting due to external forces, for such a system.

In this paper we have used the mathematics of coordinate transformations to describe the contribution of internal structural organization to flagellar mechanics. The coordinate system in which the three-dimensional structure of cilia and flagella finds its simplest representation is body coordinates. It is, of course, also possible to represent all the vectors characterizing the structure in a fixed coordinate system, in which case the appropriate fundamental variables are the Euler angles which describe finite rotations. Morgan et al. (1979) have used the Euler angles to describe the shape of a flagellum when the curvature is given. Because none of the vectors or matrices are constant in fixed coordinates, functions of the Euler angles will appear throughout the equations and render any attempts to derive the curvature from the internal mechanism cumbersome. The fact that structural quantities are constant when represented in body coordinates makes this the representation of choice. Products of matrices need be taken only after the moment balance equations are satisfied and one wishes to compute the shape. The general approach we have followed in using the coordinate transformations to develop the equilibrium equations is the one already familiar from the study of planar models (Blum and Hines, 1979), i.e., the axonemal cross section is assumed to be structurally invariant except for the arc length position of a doublet within the cross section. The problem then reduces to that of knowing the orientation of each cross section of the axoneme. The only forces of interest are then those forces that tend to change the orientation of the cross sections. Because bending moments determine orientation, a single bending moment equilibrium equation suffices to determine the shape of the entire flagellum.

This approach, which is a strict form of the sliding filament model, bypasses the question of what structures are implicated in maintaining the uniformity of each cross section by lumping the forces due to such structures under the rubric of forces of constraint and thereafter ignoring them. To deal with such forces realistically will require a highly detailed model of the properties of the dynein arms and of the radial links and central pair projections. (If the nexin links do not behave as the simple elastic elements we have assumed them to be, then a more realistic representation of their properties would also be necessary.) Conceptually, however, the procedure to be followed for elimination of the forces of constraint is straightforward. One has only to write the moment equilibrium equation for each filament separately, treating cross-bridge forces (and perhaps moments) as external forces (and moments), and solving the equilibrium equations simultaneously. In practice this is a formidable problem for even a two-filament model.

As a prerequisite for considering the contributions of such elements as nexin links, dynein cross-bridges, and the radial link system to flagellar mechanics, it is of course necessary to account for the effective resistance of the doublet microtubules themselves to bending and twisting. Use of the body coordinate transformation formalism has permitted us to show that the bend resistance matrix that is strictly applicable to a structure with the complexity of an axoneme can, to within the negligible error, be represented as a constant matrix; we have computed the principal values on the assumption that the doublets have elastic moduli appropriate for a collagenlike substance. Even so, the total bending resistance of the 10 doublets is still very small, and only one-tenth of the value used by Brokaw (1980) in his modeling studies. Okuno and Hiramoto (1979) found that the minimum effective stiffness in flagella inactivated by CO_2-saturated sea water was ~300 pN μm^2, but interpretation of their measurements is ambiguous because of contributions to stiffness that may have arisen from nexin links or radial spokes (Blum and Hines, 1979). Recent measurements of the stiffness of individual doublets (Ishijima and Hiramoto, 1982) yield a range of values for E_b from 10 to 380 pN μm^2, indicating a higher elastic coefficient for polymerized tubulin than we have used for the present computations. Okuno and Hiramoto (1979) report that after removal of a deflecting force the flagellum returns to its initial shape. Thus, purely elastic forces are probably adequate as a first approximation to the structural properties.

The relative values $E_{xx}:E_{yy}:E_{zz}$ = 1:0.9:2.2 were derived (section III) on the assumption of an idealized 9 + 2 configuration in which the central pair was treated as one outer doublet. (The absolute values, as already discussed, depend on the value of the elastic modulus.) To the extent that the central pair is more asymmetric than an outer doublet, there may be a slight increase in the disparity between E_{xx} and E_{yy} and hence in the propensity to twist under the action of an external force, but it is unlikely that this effect will be appreciable. A consequence of the sliding filament model is that pinned links between filaments contribute to shear resistance and not bending resistance. An exception to this, however, might be a permanent 5–6 cross-bridge, known to occur in some cilia. If these bridges were pinned and resisted stretch with the same high elasticity as the doublets themselves, then their effect would better be described as a substantial increase in bend resistance in the plane defined by filaments five and six and not as a very high shear resistance. Because relative sliding due to twist between outer doublets is a third-order effect

proportional to $L^3\kappa_3^3$ (section II), such a permanent 5–6 bridge would cause virtually no increase in twisting resistance and thus cannot stabilize the plane of bending. Although relative sliding between an outer doublet and the central pair is proportional to $L^2\kappa_z^2$, this is still too small to cause appreciable change in the effective twist resistance. Indeed, any structure that lies in the plane of the axonemal cross section cannot affect twist to first order because in the strict sliding filament model the axonemal cross section is invariant. If, however, cross-bridges (whether permanent 5–6 cross-bridges or other dynein arms) are rigidly attached and hence can support moments, then such links could lead to twisting. Such links are not dealt with in this paper.

The analysis presented here implies that for planar motion to occur the dynein shear force must be carefully arranged so that the net active shear force lies in a plane over the entire arc length. Several authors (Satir, 1968; Tamm and Horridge, 1970; Omoto and Kung, 1980) have proposed that the central pair may act as a commutator. Such active internal twist of one structure relative to another at a given cross section is also not dealt with in this paper.

In a strict sliding filament system containing only pinned links, twist may arise only in response to an external force that does not lie in the plane of the flagellum. If a flagellum is beating with planar motion, viscous forces will, therefore, not produce twist. If, however, fluid is made to flow normal to the plane of the flagellum, substantial twist will result. Gibbons (1975) observed that by flowing a stream of water past a flagellum in rigor, the flagellum could be twisted through 180°, and that this twist, which was reversible, could occur within a segment of flagellum as short as 3 μm in length. The speed of water flow required to produce this twist was about one-sixth that of the rate of water flow past the flagellum during normal swimming. This result could arise either because of a low twist resistance of the flagellum combined with a large torsional moment acting, for the particular shape, at the point of maximum observed twisting, or else the twist resistance at all points except those where twisting occurred was high.

Gibbons (1975) further observed that in flagella in rigor but with a normal waveform there was a twisting of ~40°–60° near each junction between a straight and curved region, and that the handedness of the twist appeared to alternate at consecutive regions, so that little or no net twist accumulated over the length of the axoneme. This cannot happen within the confines of the present model, and points to the necessity of extending the present analysis to include moment-bearing links.

Contrary to our initial intuitive belief that a sliding filament system containing only pinned links might naturally twist because of internal forces acting away from the neutral axis, the present work shows that in a strict sliding filament model internal forces cannot by themselves generate twist. Experimentally observed twisting may therefore suggest either an active twisting of the central pair in the opposite sense to that of the cylinder of the outer doublets or could result from the presence of moment bearing links.

APPENDIX

Coordinate Transformations

A thorough exposition of coordinate transformations can be found in Goldstein (1950). In this Appendix we briefly present those mathematical concepts directly relevant to this paper. A vector, $\vec{\mathbf{V}}$, specified in one coordinate system has three components, say V_x, V_y, and V_z. The same vector in another coordinate system will have different values of the components. Conversely, different vectors may have the same representation if they are expressed in terms of differing coordinate systems. This point is central to an understanding of three-dimensional motion and twist in a flagellum. Consider a coordinate system, which we designate as the x system, defined by three unit vectors $\hat{\mathbf{x}}_1$, $\hat{\mathbf{x}}_2$, $\hat{\mathbf{x}}_3$ that are orthogonal to each other. Now define a new X coordinate system with unit vectors $\hat{\mathbf{X}}_1$, $\hat{\mathbf{X}}_2$, $\hat{\mathbf{X}}_3$. The representation of the same vector in the x coordinate system can be written in terms of its representation in the x system as

$$\vec{\mathbf{V}} = \begin{pmatrix} \vec{\mathbf{V}} \cdot \hat{\mathbf{X}}_1 \\ \vec{\mathbf{V}} \cdot \hat{\mathbf{X}}_2 \\ \vec{\mathbf{V}} \cdot \hat{\mathbf{X}}_3 \end{pmatrix} = \begin{bmatrix} \hat{\mathbf{X}}_1 \cdot \hat{\mathbf{x}}_1 & \hat{\mathbf{X}}_1 \cdot \hat{\mathbf{x}}_2 & \hat{\mathbf{X}}_1 \cdot \hat{\mathbf{x}}_3 \\ \hat{\mathbf{X}}_2 \cdot \hat{\mathbf{x}}_1 & \hat{\mathbf{X}}_2 \cdot \hat{\mathbf{x}}_2 & \hat{\mathbf{X}}_2 \cdot \hat{\mathbf{x}}_3 \\ \hat{\mathbf{X}}_3 \cdot \hat{\mathbf{x}}_1 & \hat{\mathbf{X}}_3 \cdot \hat{\mathbf{x}}_2 & \hat{\mathbf{X}}_3 \cdot \hat{\mathbf{x}}_3 \end{bmatrix} \begin{pmatrix} \hat{\mathbf{V}} \cdot \hat{\mathbf{x}}_1 \\ \hat{\mathbf{V}} \cdot \hat{\mathbf{x}}_2 \\ \hat{\mathbf{V}} \cdot \hat{\mathbf{x}}_3 \end{pmatrix}. \quad \text{(A1)}$$

The elements of the 3 × 3 matrix are the direction cosines of the X system axes with respect to the x system axes. In more compact notation,

$$\vec{\mathbf{V}}^{(X)} = \underset{\approx}{\mathbf{A}}(X, x)\vec{\mathbf{V}}^{(x)}, \quad \text{(A2)}$$

where the superscript refers to the particular coordinate system in which V is represented. Transformation matrix $\underset{\approx}{\mathbf{A}}(X, x)$ transforms a vector represented from system x to system X. If we wish to transform the vector to a third coordinate system, y,

$$\vec{\mathbf{V}}^{(y)} = \underset{\approx}{\mathbf{A}}(y, X)\underset{\approx}{\mathbf{A}}(X, x)\vec{\mathbf{V}}^{(x)} = \underset{\approx}{\mathbf{A}}(y, x)\vec{\mathbf{V}}^{(x)}. \quad \text{(A3)}$$

Thus a transformation may be built from a succession of intermediate transformations (which must be carried out in the correct order, because, in general, matrices do not commute).

From Eq. A1 it can be seen that the inverse transformation is given by the transpose of the matrix, i.e., this orthogonal condition provides six independent relations among the direction cosines of the transformation matrix. Thus three quantities suffice to determine a coordinate transformation. This fact finds expression in Euler's theorem that states that any proper transformation is a rotation about some axis (see Goldstein, 1950, for further details). The three quantities that specify a finite transformation do not form a vector. A vector can, however, be associated with infinitesimal transformations.

The transformation from body coordinates at s to body coordinates at $s + ds$ can be written as an infinitesimal rotation about the x axis by angle $d\theta$, followed by an infinitesimal rotation about the y axis by $d\phi$ and then about the z axis, by $d\psi$. (The general form of a rotation about the x axis, e.g., is

$$\begin{bmatrix} 1 & 0 & 0 \\ 0 & \cos\theta & \sin\theta \\ 0 & -\sin\theta & \cos\theta \end{bmatrix}. \quad \text{(A4)}$$

For infinitesimal rotations, the cosine terms become 1 and the sine terms become $d\theta$.) Note that the order of the rotations is not important because infinitesimal transformations commute. Multiplication of the three in-

finitesimal rotation matrices (omitting higher-order terms) yields a matrix that can be written as

$$\underset{\approx}{A}(s,s+ds) = 1 + ds\begin{bmatrix} 0 & \kappa_z & -\kappa_y \\ -\kappa_z & 0 & \kappa_x \\ \kappa_y & -\kappa_x & 0 \end{bmatrix}, \qquad \text{(A5)}$$

where $\kappa_x = d\theta/ds$, $\kappa_y = d\phi/ds$, and $\kappa_z = d\psi/ds$. It turns out that the components of the matrix in Eq. A5 transform as the components of a vector under proper rotations. For example, the vector

$$\underset{\approx}{\kappa}\vec{V} = \begin{pmatrix} \kappa_z V_y - \kappa_y V_z \\ \kappa_x V_z - \kappa_z V_x \\ \kappa_y V_x - \kappa_x V_y \end{pmatrix} \qquad \text{(A6)}$$

has the same components as the vector cross product $-\vec{\kappa} \times \vec{V}$. Now consider the derivative with respect to arc length of a vector

$$\frac{d\vec{V}}{ds} = \lim_{\Delta s \to 0} \frac{\vec{V}(s+\Delta s) - \vec{V}(s)}{\Delta s}. \qquad \text{(A7)}$$

The indicated subtraction can be performed only when the two vectors are represented in the same coordinate system. Suppose that $V_i(s)$ and $V_i(s + \Delta s)$, with $i = 1, 2, 3$, are the representations of $\vec{V}$ in body coordinates at s and $s + \Delta s$, respectively. Then the representation of Eq. A7 in body coordinates at s is

$$\frac{d\vec{V}}{ds_i} = \lim_{\Delta s \to 0} \frac{A_{ij}(s, s+\Delta s)V_j(s+\Delta s) - V_i(s)}{\Delta s}. \qquad \text{(A8)}$$

Note that the left-hand side is the ith component in body coordinates at s of the vector $d\vec{V}/ds$. Now, using Eq. A5, we have

$$\frac{dV}{ds_1} = \frac{dV_i}{ds} - \kappa_{ij}V_j. \qquad \text{(A9)}$$

Returning to vector notation yields Eq. 1 of the text.

This work was supported by National Institutes of Health grant NS11613. We are grateful to Dr. Y. Hiramoto for permission to use unpublished data.

Received for publication 26 March 1982 and in revised form 16 August 1982.

REFERENCES

Blum, J. J., and M. Hines. 1979. Biophysics of flagellar motility. *Q. Rev. Biophys.* 12:104–180.

Bradfield, J. R. G. 1955. Fiber patterns in animal flagella and cilia. *Symp. Soc. Exp. Biol.* 9:306–334.

Brokaw, C. J. 1980. Theoretical models for oscillation and bend propagation by sperm flagella. *In* Testicular Development, Structure, and Function. A. Steinberger and E. Steinberger, editors. Raven Press, New York. 447–453.

Costello, D. P. 1973. A new theory on the mechanics of ciliary and flagellar motility. II. Theoretical considerations. *Biol. Bull.* 145:292–309.

Costello, D. P., C. Henley, and C. R. Ault. 1969. Microtubules in spermatozoa of *Chilidia (Turbellaria, Acoela)* revealed by negative staining. *Science (Wash. D.C.).* 163:678–679.

Crandall, S. H., and N. C. Dahl. 1959. An Introduction to the Mechanics of Solids. McGraw-Hill, Inc., New York. 244.

Crowley, P. H., C. J. Benham, S. M. Lenhart, and J. L. Morgan. 1981. Peripheral doublet microtubules and wave generation in eukaryotic flagella. *J. Theor. Biol.* 93:769–784.

Gibbons, I. R. 1975. The molecular basis of flagellar motility in sea urchin spermatozoa. *In* Molecules and Cell Movement. S. Inoue and R. E. Stephens, editors. Raven Press, New York. 207–231.

Goldstein, H. 1950. Classical Mechanics. Addison-Wesley, Reading. 93–140.

Goldstein, S. F., C. Besse, and J. Schrevel. 1978. Structure and physiology of a "6 + 0" flagellum. Abstracts, U.S.-Japan Science Seminar on Mechanism and controls of prokaryotic and eukaryotic flagellar motility, Hakone. 21.

Gray, J., and G. J. Hancock. 1955. The propulsion of sea urchin spermatozoa. *J. Exp. Biol.* 32:802–814.

Henley, C., D. P. Costello, M. B. Thomas, and W. D. Newton. 1969. The "9 + 1" pattern of microtubules in spermatozoa of mesostoma (*Platyhelminthes, Turbellaris*). *Proc. Natl. Acad. Sci. U.S.A.* 64:849–856.

Hines, M., and J. J. Blum. 1978. Bend propagation in flagella. I. Derivation of equations of motion and their simulation. *Biophys. J.* 23:41–57.

Hines, M., and J. J. Blum. 1979. Bend propagation in flagella. II. Incorporation of dynein cross-bridge kinetics into the equations of motion. *Biophys. J.* 25:421–441.

Hines, M., and J. J. Blum. 1982. Three dimensional ciliary mechanics. *Cell Motil. Suppl.* 1:153–158.

Holwill, M. E. J., H. J. Cohen, and P. Satir. 1979. A sliding microtubule model incorporating axonemal twist and compatible with three dimensional ciliary bending. *J. Exp. Biol.* 78:265–280.

Ishijima, S., and Hiramoto, Y. 1982. Mechanical properties of sperm flagella. *Cell. Motil. Suppl.* 1:149–152.

Lubliner, J. 1973. An analysis of interfilament shear in flagella. *J. Theor. Biol.* 41:119–125.

Lubliner, J., and J. J. Blum. 1971. Model for bend propagation in flagella. *J. Theor. Biol.* 31:1–24.

Morgan, J. L., P. H. Crowley, C. J. Benham, T. L. Hayden, and S. M. Lenhart. 1979. Model for wave generation by eukaryotic flagella. *J. Cell Biol.* 83(2 Pt. 2):177*a* (Abstr.).

Okuno, M., and Y. Hiramoto. 1979. Direct measurements of the stiffness of echinoderm sperm flagella. *J. Exp. Biol.* 79:235–243.

Omoto, C. K., and C. Kung. 1980. Rotation and twist of the central-pair microtubules in the cilia of *Paramecium*. *J. Cell Biol.* 87:33–46.

Prensier, G., E. Vivier, S. Goldstein, and J. Schrevel. 1979. Motile flagellum with a "3 + 0" ultrastructure. *Science (Wash. D.C.)* 207:1493–1494.

Satir, P. 1968. Studies on cilia. III. Further studies on the cilium tip and a "sliding filament model" of ciliary motility. *J. Cell Biol.* 39:77–94.

Schreiner, K. E. 1977. Displacement and sliding of twisted filaments in cilia and flagella. *J. Biomech.* 10:1–4.

Schrevel, J., and C. Besse. 1975. Un type flagellaire fonctionnel de base 6 + 0. *J. Cell Biol.* 66:492–507.

Tamm, S. L., and G. H. Horridge. 1970. The relation between the orientation of the central fibrils and the direction of beat in cilia of *Opalina*. *Proc. R. Soc. Lond. B. Biol. Sci.* 175:219–233.

Warner, F. D. 1978. Cation-induced attachment of ciliary dynein cross-bridges. *J. Cell Biol.* 77:R19–R26.

Warner, F. D., and P. Satir. 1974. The structural basis of ciliary bend formation: Radial spoke positional changes accompanying microtubule sliding. *J. Cell Biol.* 63:35–63.

Wooley, D. M. 1977. Evidence for "twisted plane" undulations in golden hamster sperm tails. *J. Cell Biol.* 75:851–865.